Scripta Materialia 190 (2021) 108–112

Contents lists available at ScienceDirect

Scripta Materialia

journal homepage: www.elsevier.com/locate/scriptamat

Hydrogen-enhanced densified twinning (HEDT) in a twinning-induced plasticity (TWIP) steel

Cheng Zhang[a,b], Huihui Zhi[a,b], Stoichko Antonov[c], Lin Chen[a,b], Yanjing Su[a,b,*]

[a] Beijing Advanced Innovation Center for Materials Genome Engineering, University of Science and Technology Beijing, Beijing 100083, PR China
[b] Corrosion and Protection Center, University of Science and Technology Beijing, Beijing 100083, PR China
[c] Department of Microstructure Physics and Alloy Design, Max-Planck-Institut für Eisenforschung GmbH, Düsseldorf 40237, Germany

ARTICLE INFO

Article history:
Received 1 July 2020
Revised 26 August 2020
Accepted 27 August 2020
Available online 4 September 2020

Keywords:
Austenitic steels
Twinning
Dislocations
Hydrogen embrittlement

ABSTRACT

The effect of hydrogen on the twinning evolution in a twinning-induced plasticity (TWIP) austenitic steel was investigated at different strain levels. The presence of hydrogen decreased the twin thickness and increased the twin density in individual twin bundles, in comparison with the hydrogen-free condition. This mechanism, reported for the first time, was termed hydrogen-enhanced densified twinning (HEDT). Based on these experimental observations, the effect of hydrogen on twinning was analyzed from the three stages of nucleation, growth and stability. HEDT may elevate the local stress, and thus significantly affect the hydrogen embrittlement (HE) of TWIP steels.

High-Mn, austenitic, twinning-induced plasticity (TWIP) steels have experienced wide research interest in recent years due to their excellent mechanical properties, such as high strength and high ductility [1,2]. Numerous studies have reported that this desirable combination of mechanical properties originates from the formation of a high density of deformation twins, which act as strong obstacles against dislocation movement [3–8]. Particularly, Sevillano [9,10] reported that the whisker-like, nano-scale, thin twins act as hard inclusions, resulting in a "composite strengthening" effect in TWIP steels. Furthermore, Idrissi et al. [11] showed that TWIP steels with finer twins possess superior work-hardening capability when compared to other cases of nearly the same twin volume fraction.

There are multiple factors affecting the twin thickness, including temperature [12,13], strain-rate [6,14], stress state [15,16], stacking fault energy (SFE) [17], etc. Bal et al. [18] observed that the presence of hydrogen decreases the twin thickness, and the decreased twin thickness promotes hydrogen embrittlement (HE), which is contrast to abovementioned reports that steels with finer twins have greater mechanical property [9–11]. Some studies have proposed that this deteriorated property might be due to the high stress concentration at the twin junctions [19,20], which facilitates high hydrogen concentration at the twin boundaries or within the twins [20]. Thus, the twin boundaries act as crack initiation sites [18,21] as well as propagation paths [20] in TWIP steels under hydrogen environment. Nevertheless, there is lack of knowledge on the evolution of deformation twin characteristics, such as the thickness or distribution, under the effect of a hydrogen-rich environment. Therefore, the aim of this study is to elucidate the effect of hydrogen on the twinning evolution, in order to further understand the HE phenomenon of TWIP steels. Here, a hydrogen-enhanced densified twinning (HEDT) mechanism is proposed for the first time based on electron backscattered diffraction (EBSD) and transmission electron microscope (TEM) observations of individual twins and twin bundles in hydrogen-free and hydrogen-charged samples.

Fe-22Mn-0.6C TWIP steel with a SFE of about 19 mJ/m^2 [22] was used in this study; chemical composition listed in Table 1. The ingot weighting 20 kg was homogenized at 1423 K for 2 hours in a protective gas atmosphere, hot-rolled to 3 mm at no less than 1223 K, and cold-rolled to a 1.5 mm thick plate. Samples were excised and annealed at 1173 K for 15 min followed by water quenching to prevent carbide precipitation during cooling.

Dog-bone tensile specimens with gauge dimensions of 20 mm × 5 mm × 1.5 mm were prepared with the tensile axis parallel to the rolling direction. The tensile specimens were electrochemically charged with hydrogen in a 3% NaCl aqueous solution containing 0.3 g/L NH_4SCN at room temperature with a current density of 50 A/m^2 for 48 h. A platinum wire was used as the counter-electrode. Slow strain-rate tensile (SSRT) tests of the hydrogen-free (H-free) and hydrogen-charged (H-charged) tensile specimens were carried out at room temperature with a constant crosshead speed of 0.012 mm/min (corresponding to an ini-

* Corresponding author.
E-mail address: yjsu@ustb.edu.cn (Y. Su).

https://doi.org/10.1016/j.scriptamat.2020.08.047
1359-6462/

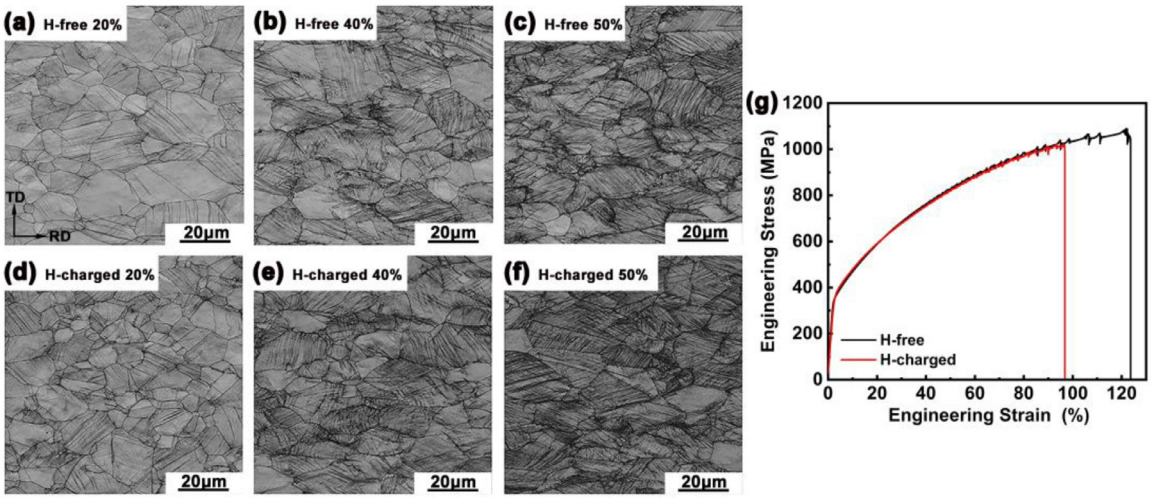

Fig. 1. EBSD-KPQ maps at (a) ε = 20%, (b) ε = 40%, and (c) ε = 50% of the H-free tensile specimens and (d) ε = 20%, (e) ε =40% and (f) ε = 50% of the H-charged tensile specimens; (g) Engineering stress-strain curve.

Table 1
Chemical compositions (wt.%) of the TWIP steel used in the present study.

TWIP steel	Mn	C	Fe
Fe-22Mn-0.6C	21.26	0.55	Bal.

Table 2
Compensation factor (k) for the H-free and H-charged specimens at different strain levels

Specimen Condition	Strain Level (%)		
	20	40	50
H-free (k)	0.23	0.38	0.44
H-charged (k)	0.25	0.43	0.46

tial strain rate of 1 × 10^{-5} /s). During the SSRT, the specimens were interrupted at different strain levels for microstructural observations.

Deformation twins were observed using EBSD (Tescan mira 3 LMH) and TEM (Tecnai G20). The specimens for EBSD observations were mechanically polished and subsequently electropolished in a 15% perchloric acid and 85% acetic acid solution. EBSD maps were acquired using the step size of 0.15 μm. Due to the thinness of the hydrogen-affected regions (~ 40 μm) arising from the slow hydrogen diffusion in austenite [23,24], the TEM specimens were taken from the surface of the tensile specimen's gauge by grinding from the inter-region towards the surface, thereby obtaining a specimen from the hydrogen-affected zone. The TEM specimens of the H-free steels were also taken from the same position in order to eliminate the influence of the stress state. The thin foils were further prepared by twin-jet polishing, which was performed at 288 K with an applied potential of 20 V in a mixed solution of 90% glacial acetic acid and 10% perchloric acid.

The recrystallized, equiaxed grain size of the presented steels was ~8 μm. The EBSD Kikuchi pattern quality (KPQ) maps [3,25] of the H-free and H-charged specimens at different strains are shown in Fig. 1(a–f). The twin volume fraction, which is defined as the area of deformation twins per observed area, generally increased with strain irrespective of the hydrogen content. Fig. 1(g) shows the engineering stress-strain curves of H-free and H-charged specimens, where it can be seen that the hydrogen significantly decreased the ultimate tensile strength and elongation.

Due to the inherently lower resolution of EBSD KPQ maps with respect to feature size, only twin bundles consisting of several individual twins can be observed by this technique [3,26], leading to overestimation of the twin volume fraction. In contrast, TEM, which has sufficient resolution, has a limited observation area. Therefore, we utilized a combination of EBSD and TEM observations to compensate for each method's respective shortcomings [27]. The twin volume fraction per unit area was determined by point counting analysis based on EBSD data, which covers an area of ~13,000 μm^2 for a given strain. The reliability of this method has been evaluated [28,29]. Meanwhile, the twin thickness, λ, and spacing between the adjacent twins, δ, in the bundles were measured by TEM [3,26], and a compensation factor (k), given by Eq. (1), was used to revise the EBSD results.

$$k = \frac{\lambda}{\lambda + \delta} \tag{1}$$

TEM dark-field (DF) images (Fig. 2(a, b)) of the H-free and H-charged specimens at 50% strain show several, representative, individual twins with 2-70 nm thickness. At least 200 such twins were considered for each condition, and the results are provided in Fig. 2. As shown in Fig. 2(c, d), the average twin thickness did not change with respect to strain, but the presence of hydrogen reduced it from 29 nm to 21 nm. Meanwhile, the twin spacing gradually decreased with the increasing strain (Fig. 2(e, f)), and again hydrogen reduced the average twin spacing. The variations in average individual twin thickness and twin spacing with respect to strain are plotted in Fig. 2(g). With increased strain, the twin spacing gradually approaches the thickness thus the compensation factor (k) shown in Table 2 approximately increases to 0.5. The twin volume fraction at any strain level of the H-charged specimen was higher compared to the H-free specimen (Fig. 2(h)) and all of them relatively saturated at 50% strain.

Statistical analysis of at least 150 twin bundles at 50% strain, shown in Fig. 3(a, b) revealed that the spacing between twin bundles was reduced from 246 nm in the H-free specimen to 183 nm in H-charged specimen, whereas the twin bundle thickness distribution in both specimens remained equivalent, with an average of ~310 nm. Nevertheless, the TEM analysis revealed that the individual twin thickness in the H-charged sample is finer, and therefore, we unveil a hydrogen effect on TWIP steels, i.e. there are more twins generated in an individual bundle with similar thickness and compensation factor (k) in the H-charged condition compared to

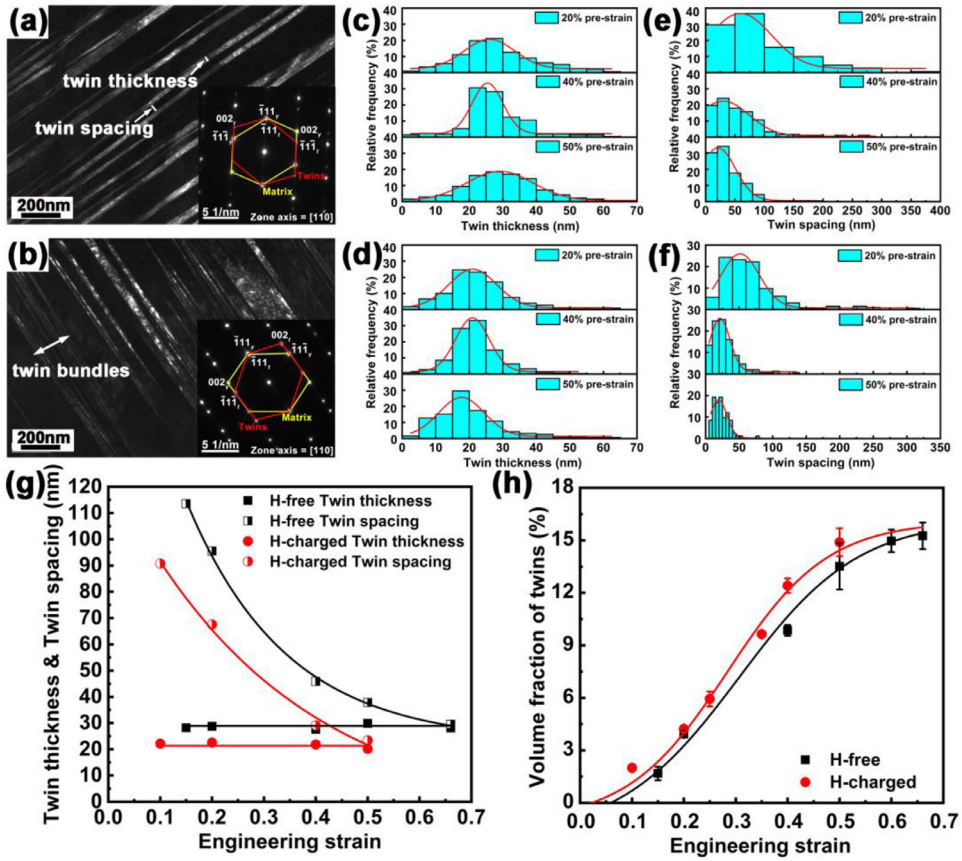

Fig. 2. TEM-DF images of (a) H-free and (b) H-charged specimens at a strain of 50% showing the mechanical twins; Statistical distributions of individual twin thickness (c, d) and spacing (e, f) in H-free and H-charged specimens, respectively, at different strains (20%, 40% and 50%); (g) Variations in the average twin thickness (λ) and twin spacing (δ); and (h) Twin volume fraction with respect to strain in the H-free and H-charged specimens.

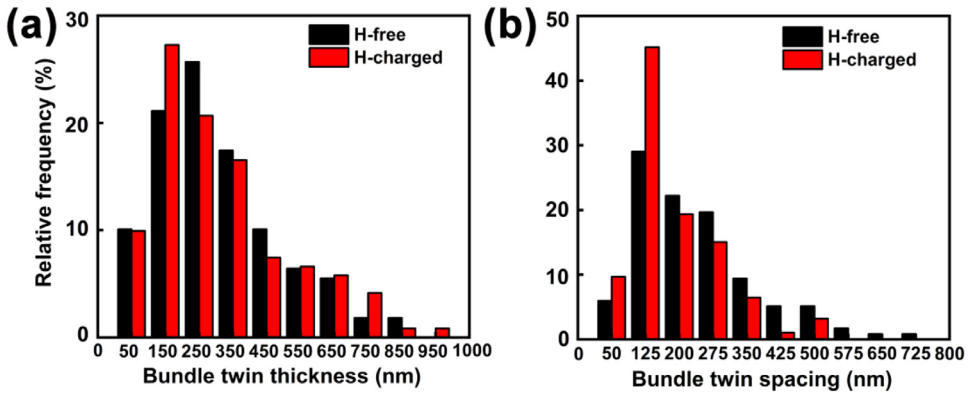

Fig. 3. Statistical distributions of twin bundle (a) thickness and (b) spacing in the H-free and H-charged specimens at 50% strain.

H-free one. Maintaining convention, we term this novel mechanism as hydrogen-enhanced densified twinning (HEDT).

The evolution of deformation twins includes nucleation, growth and stable states, as schematically shown in Fig. 4. Several twinning mechanisms [30–33] have been previously proposed depending on the material and/or deformation conditions, hence there is still no universal twin nucleation process. Although dislocation dissociation reactions influence twin formation, Shockley partial dislocations are of particular importance in different models. In this study, we explain the effect of hydrogen on the twin nucleation process based upon the model of Cohen and Weertman [31]. The model includes dissociation of perfect dislocations into Shockley partial dislocations on the primary plane or conjugate plane (Eq. (2)) and dissociation of perfect dislocations into sessile Frank partial dislocations and glissile Shockley partial dislocations on the conjugate plane when encountering an L-C barrier (Eq. (3)) as depicted in Fig. 4(a).

$$\frac{a}{2}[10\bar{1}]=\frac{a}{6}[11\bar{2}]+\frac{a}{6}[2\bar{1}\bar{1}] \tag{2}$$

$$\frac{a}{2}[011]_{(11\bar{1})}=\frac{a}{3}[111]+\frac{a}{6}[\bar{2}11]_{(111)} \tag{3}$$

According to Eq. (2), the equilibrium spacing between two Shockley partial dislocations is a balance of the repulsive force between the dislocations and the attractive force due to the formation of a stacking fault (SF). In order to stabilize the stacking fault

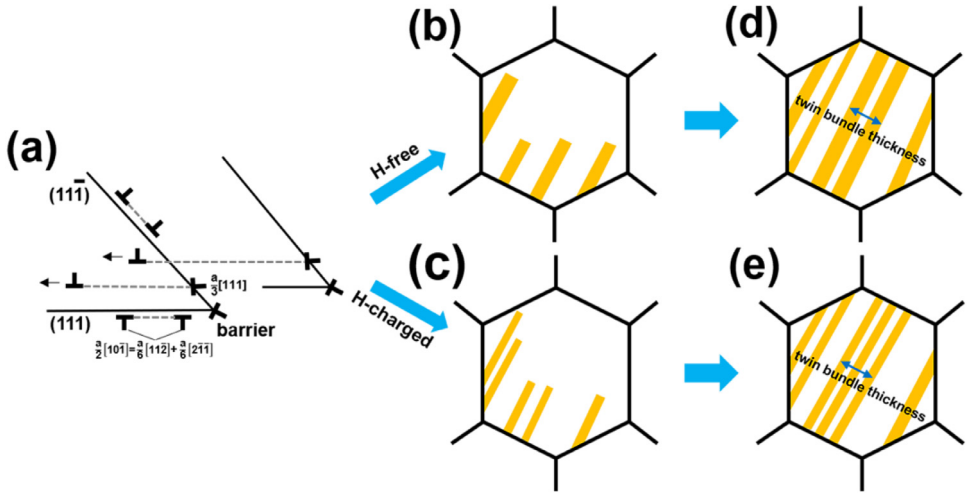

Fig. 4. Schematic illustration of the influence of hydrogen on twinning evolution at different strain stages of the TWIP steel: (a) nucleation state; (b, c) growth state; (d, e) stable state. Note that the thin bands represent twins, and the twin bundles are indicated by two-way arrows.

and develop a twin, Byun [34] proposed an idea of infinite separation. The critical twinning stress is equivalent to the applied force needed to make the distance between partial dislocations infinite, that is when the external stress reaches $2\gamma_{SF}/b_p$ (γ_{SF} represents the SFE and b_p represents burgers vector of partial dislocation). Thus, due to the reduction of the SFE by hydrogen [35,36], the decreased critical stress facilitates easier twin nucleation.

From Eq. (3), since the energy before and after the reaction is equivalent, a sufficiently large external stress is needed to emit the Shockley partial dislocations. Many researchers [37–39] have developed their models based on the different forces acting on the Shockley partial dislocations. The critical stress can be expressed as:

$$\tau_T = \tau(SFE) + \tau(interactions) - \tau(pile-up) \tag{4}$$

First, $\tau(SFE)$ is proportional to the SFE, so the addition of hydrogen reduces $\tau(SFE)$ [40,41]. Second, due to the shielding effect of hydrogen [42], the interaction energy between dislocations and obstacles (other dislocations, twin boundaries, etc.) reduces. Thus, the enhanced dislocation mobility results in a reduction of the second term of Eq. (4). Finally, on the one hand, the dislocation density increases due to the presence of hydrogen [42,43], while on the other, the mathematical derivation of Jiang et al. [44] shows that hydrogen attracts the dislocations emitted from the dislocation source to pile-up around obstacles, resulting in an increased dislocation density in pile-up groups, which increases $\tau(pile-up)$ [30]. In general, hydrogen reduces the critical twinning stress by affecting the dislocation dynamics. Therefore, the increase of twin nucleation sites in the H-charged condition leads to an increase in the twin volume fraction and a reduction of the twin spacing, as schematized in Fig. 4(b, c).

Furthermore, only when the twin embryo thickness is larger than the critical thickness (λ_c), a stable twin can be formed under the driving force. The relationship between the critical thickness and driving stress (σ) can be expressed as [45]:

$$\lambda_c = \frac{5\pi}{4}\frac{G\gamma_{TB}}{\sigma^2} \tag{5}$$

where G is the shear modulus and γ_{TB} is the twin boundary energy (proportional to the SFE). The driving stress can be regarded as the stress at the pile-up at the boundaries. As explained before, because of the increase in the driving stress and reduction of the SFE in the H-charged specimens, its λ_c is smaller than in the H-free condition (Fig. 4(b, c)). Additionally, the twin growth is limited by sessile dislocations located at the twin boundaries to maintaining thickness and stability [11]. So, the growth should be similar under the same deformation conditions and the twin thickness remains unchanged as the strain increases. Consequently, twinning densified occurs in H-charged specimens such that more and finer twins form in a twin bundle (Fig. 4(d, e)).

Based on the composite strengthening theory proposed by Gil Sevillano [9,10], the flow stress at any strain (ε) can be estimated as:

$$\sigma = \left[1 - f_V^T\right]\sigma_M + \beta f_V^T \sigma_T \tag{6}$$

where σ is the macroscopic flow stress, f_V^T is the twin volume fraction, σ_M is the strength of the matrix, β is a constant, and σ_T is the strength of the thin twin (which has negative correlation with the twin thickness). When Eq. (6) is applied to the twin bundles for the two specimens at 50% strain, f_V^T is about 0.5, but the finer twins in the H-charged specimen leads to an increase in σ_T. Thus, the local stress of the twin bundles increases, which can also be a cause of crack nucleation and HE.

In summary, the effects of hydrogen on the twinning evolution in a Fe-22Mn-0.6C TWIP steel was investigated by combined EBSD and TEM observations at different strains. Compared to the H-free specimens, the hydrogen reduced the twin thickness in the H-charged specimens. The increased nucleation sites of twins resulted in an increase of the twin volume fraction in the H-charged specimens. Meanwhile, the twin spacing was gradually reduced to be similar to the twin thickness when the strain was around 50%. More nucleation sites and finer twins result in overall more twins in the individual twin bundles of the H-charged condition, compared to twin bundles of similar thickness in the H-free samples. This phenomenon, termed “hydrogen-enhanced densified twinning (HEDT)”, could lead to higher local stress concentrations in the twin bundles, which is of great significance for HE of TWIP steel.

Declaration of Competing Interest

The authors declare that they have no known competing financial interests or personal relationships that could have appeared to influence the work reported in this paper.

Acknowledgments

This work was supported by the National Key R&D Program of China (2016YFB0300204), the National Key R&D Program of

China (2016YFB0700505), the National Natural Science Foundation of China (51571028) and the 111 Project (B170003).

Supplementary materials

Supplementary material associated with this article can be found, in the online version, at doi:10.1016/j.scriptamat.2020.08.047.

References

[1] O. Bouaziz, S. Allain, C.P. Scott, P. Cugy, D. Barbier, Curr. Opin. Solid St. M. 15 (2011) 141–168.
[2] H.H Zhi, C. Zhang, Z. Guo, S. Antonov, Y.J. Su, Materials 13 (2020) 1184.
[3] K. Jeong, J.E. Jin, Y.S. Jung, S. Kang, Y.K. Lee, Acta Mater. 61 (2013) 3399–3410.
[4] H.K. Yang, Z.J. Zhang, Z.F. Zhang, Scripta Mater. 68 (2013) 992–995.
[5] H.K. Yang, Z.J. Zhang, F.Y. Dong, Q.Q. Duan, Z.F. Zhang, Mater. Sci. Eng. A. 607 (2014) 551–558.
[6] H.K. Yang, Z.J. Zhang, Z.F. Zhang, Mater. Sci. Eng. A. 622 (2015) 184–188.
[7] Y.F. Shen, L. Lu, Q.H. Lu, Z.H. Jin, K. Lu, Scripta Mater. 52 (2005) 989–994.
[8] L. Lu, Z.S. You, K. Lu, Scripta Mater. 66 (2012) 837–842.
[9] J.G. Sevillano, Scripta Mater. 60 (2009) 336–339.
[10] J.G. Sevillano, F.D.L. Cuevas, Scripta Mater. 66 (2012) 978–981.
[11] H. Idrissi, K. Renard, D. Schryvers, P.J. Jacques, Scripta Mater. 63 (2010) 961–964.
[12] Y.H. Fan, F. Cui, L. Lu, B. Zhang, J Alloy Compd. 788 (2019) 1066–1075.
[13] G.H. Xiao, N.R. Tao, K. Lu, Scripta Mater. 59 (2008) 975–978.
[14] H.K. Yang, Z.J. Zhang, Y.Z. Tian, Z.F. Zhang, Mater. Sci. Eng. A 690 (2017) 146–157.
[15] K. Renard, H. Idrissi, D. Schryvers, P.J. Jacques, Scripta Mater. 66 (2012) 966–971.
[16] T. Niendorf, C. Lotze, D. Canadinc, A. Frehn, H.J. Maier, Mater. Sci. Eng. A 499 (2009) 518–524.
[17] Y. Zhang, N.R. Tao, K. Lu, Scripta Mater. 60 (2009) 211–213.
[18] B. Bal, M. Koyama, G. Gerstein, H.J. Maier, K. Tsuzaki, Int. J. Hydrogen Energ. 41 (2016) 15362–15372.
[19] P. Müllner, C. Solenthaler, P.J. Uggowitzer, M.O. Speidel, Acta Metall. Et. Mater. 42 (1994) 2211–2217.
[20] M. Koyama, E. Akiyama, K. Tsuzaki, D. Raabe, Acta Mater. 61 (2013) 4607–4618.
[21] M. Koyama, E. Akiyama, T. Sawaguchi, D. Raabe, K. Tsuzaki, Scripta Mater. 66 (2012) 459–462.
[22] A. Dumay, J.P. Chateau, S. Allain, S. Migot, O. Bouaziz, Mater. Sci. Eng. A. 483-484 (2008) 184–187.
[23] M. Koyama, E. Akiyama, K. Tsuzaki, Corros. Sci. 59 (2012) 277–281.
[24] M. Koyama, E. Akiyama, K. Tsuzaki, Corros. Sci. 54 (2012) 1–4.
[25] J.E. Jin, Y.K. Lee, Mater. Sci. Eng. A. 527 (2009) 157–161.
[26] J.K. Hwang, I.C. Yi, I.H. Son, J.Y. Yoo, B. Kim, A. Zargaran, N.J. Kim, Mater. Sci. Eng. A. 644 (2015) 41–52.
[27] H.H. Zhi, C. Zhang, S. Antonov, H.Y. Yu, T. Guo, Y.J. Su, Acta Mater. (2020).
[28] K. Renard, P.J. Jacques, Mater. Sci. Eng. A. 542 (2012) 8–14.
[29] J.E. Jung, J. Park, J.S. Kim, J.B. Jeon, S.K. Kim, Y.W. Chang, Met. Mater. Int. 20 (2014) 27–34.
[30] J.A. Vbnablbs, J. Mech. Phys. Solids 25 (1964) 693–700.
[31] J.B. Cohen, Acta Metall. 11 (1963) 996–998.
[32] T. Mori, H. Fujita, Acta Metall. 28 (1980) 771–776.
[33] S. Mahajan, G.Y. Chin, Acta Metall. (1973) 21.
[34] T.S. Byun, Acta Mater. 51 (2003) 3063–3071.
[35] P.J. Ferreira, I.M. Robertson, H.K. Birnbaum, Mater. Sci. Forum 207-209 (1996) 93–96.
[36] A.E. Pontini, J.D. Hermida, Scripta Mater. 37 (1997) 1831–1837.
[37] I. Karaman, H. Sehitoglu, K. Gall, Y.I. Chumlyakov, H.J. Maier, Acta Mater. 48 (2000) 1345–1359.
[38] I. Karaman, H. Sehitoglu, H.J. Maier, Y.I. Chumlyakov, Acta Mater. 49 (2001) 3919–3933.
[39] I. Karaman, H. Sehitoglu, Y.I. Chumlyakov, H.J. Maier, I.V. Kireeva, Scripta Mater. 44 (2001) 337–343.
[40] M. Ghasri-Khouzani, J.R. McDermid, Mater. Sci. Eng. A. 621 (2015) 118–127.
[41] K. Yamada, M. Koyama, T. Kaneko, K. Tsuzaki, Scripta Mater. 105 (2015) 54–57.
[42] P. Sofronis, Y. Liang, N. Aravas, Eur. J. Mech. A-Solid 20 (2001) 857–872.
[43] I.M. Robertson, Eng. Fract. Mech. 68 (2001) 671–692.
[44] J.S. Rui, D.L. Peng, Struct. Environ. Eng. (1994).
[45] M.A. Meyers, O. Vöhringer, V.A. Lubarda, Acta Mater. 49 (2001) 4025–4039.